ACS APPLIED MATERIALS & INTERFACES

Research Article

www.acsami.org

Antibacterial Activity of Silver Doped Titanate Nanowires on Ti Implants

Ziqiang Xu,[‡,⊥] Man Li,[‡,⊥] Xia Li,[‡] Xiangmei Liu,[*,‡] Fei Ma,[†] Shuilin Wu,[*,‡] K. W. K. Yeung,[§] Yong Han,[*,†] and Paul K. Chu[∥]

[†]State Key Laboratory for Mechanical Behavior of Materials, School of Materials Science and Engineering, Xi'an Jiaotong University, Xi'an, Shaanxi, 710049, China

[‡]Hubei Collaborative Innovation Center for Advanced Organic Chemical Materials, Ministry-of-Education Key Laboratory for the Green Preparation and Application of Functional Materials, Hubei Key Laboratory of Polymer Materials, School of Materials Science & Engineering, Hubei University, Wuhan, 430062, China

[§]Division of Spine Surgery, Department of Orthopaedics & Traumatology, Li KaShing Faculty of Medicine, The University of Hong Kong, Hong Kong, 999077, China

[∥]Department of Physics & Materials Science, City University of Hong Kong, Tat Chee Avenue, Kowloon, Hong Kong, 999077, China

Supporting Information

ABSTRACT: A nanostructured film composed of one-dimensional titanate nanowires (TNWs) was employed as a carrier of Ag nanoparticles and chitosan (CS) to improve the surface antibacterial activity and biocompatibility of titanium implants. A TNWs film was produced on a Ti substrate by an alkali hydrothermal reaction and subsequently doped by Ag nanoparticles through an ultraviolet light chemical reduction. The CS nanofilm was deposited on the Ag nanoparticles through a spin-assisted layer by layer assembly method. The results disclosed that Ag nanoparticles were successfully carried by TNWs and homogeneously distributed on the entire surface. Moreover, a CS nanofilm was also successfully deposited on the Ag nanoparticles. Antibacterial tests showed that the samples modified with a higher initial concentration of $AgNO_3$ solution exhibited better antibacterial activity, and that a CS nanofilm could further improve the antibacterial activity of the TNWs. Cell viability and ALP tests revealed that the release of Ag^+ was detrimental for the growth, proliferation, and differentiation of MC3T3, and that CS could lower the negative effects of Ag gradually as the incubation time increased.

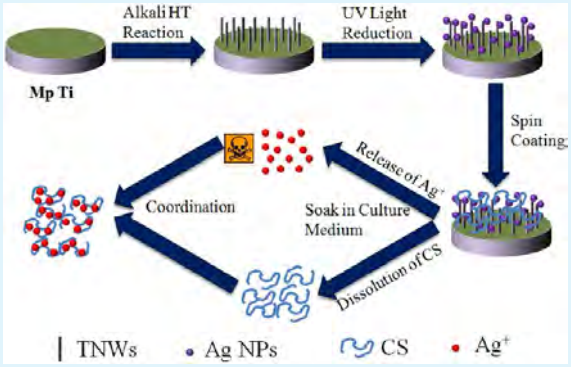

KEYWORDS: *nanostructured film, nanowire, Ag nanoparticle, antibacterial, titanium, implant*

1. INTRODUCTION

Titanium (Ti) based alloys are standard biomaterials used extensively in the field of orthopedics and dentistry due to their desirable properties, such as corrosion resistance, better mechanical properties, and good biocompatibility.[1] Moreover, compared with human bone, they also possess superior fatigue strength, high wear resistance, and similar Young's modulus.[2]

Although they can support weight and are biocompatible, it often takes a long time to form new bone tissues to directly contact with an implant due to their bioinert nature.[3] Fortunately, some surface techniques can be employed to improve the biological properties of Ti-based metallic implants and enhance the osteointegration as well as retain their favorable mechanical properties.[4−6] The surface modifications can be achieved through different methods, such as sol−gel,[7] sputtering,[8] electrophoretic,[9] chemical vapor deposition,[10] anodization,[11] and hydrothermal methods.[12−14] Among these reported methods, a hydrothermal process is often utilized to functionalize the surface of biomaterials due to the facile route to prepare one-dimensional nanomaterials on the substrate despite the shape and topography.[15]

Although bioactivity can be improved by the methods mentioned above, bacterial attachment will cause a deleterious effect on the result and success ratio of Ti-based implants.[16,17] In order to avoid infection, it is necessary to endow Ti-based implants with self-antibacterial ability. Therefore, surface modification by incorporating with antibacterial agents to inhibit the adhesion of bacteria and microbes on the Ti-based implants should an effective route to enhance the success ratios of clinical treatments for Ti-based metallic implants.[18−21] Ti-based implants have been endowed with self-antibacterial properties via various strategies which include titanate nano-

Received: April 7, 2016
Accepted: June 14, 2016
Published: June 23, 2016

DOI: 10.1021/acsami.6b04161
ACS Appl. Mater. Interfaces 2016, 8, 16584−16594

wires (TNWs) loaded with antibiotics,[22,23] inorganic bactericide doped TNWs,[24−26] bioactive antibacterial polymerization,[27,28] nonantibiotic organic bactericide loaded TNWs,[29,30] and adhesion-resistant TNWs.[31]

However, the fast release of the antibacterial agent would cause safety concerns, and the emergence of resistance strains is another issue when excessive antibiotics are administered.[32] Compared with antibiotics, silver (Ag) is a nonspecific and inorganic bactericide agent that displays an obvious effect on a broad spectrum of microbial species. Ag is also attractive on account of the good stability in the physiological environment and the difficulty to develop resistant strains.[33,34] So Ag has always been used as a bactericide to cure various infection related diseases, and it was also employed as an antiseptic and antimicrobial agent against different bacteria (Gram-positive and Gram-negative) due to its low cytotoxicity in the past.[35] In recent years, Ag nanoparticles are very attractive to be adopted as inorganic antimicrobial agents. This will open up a whole new direction to fight against a series of bacterial pathogens.[36] Moreover, Huang et al. have reported that Ag nanoparticles have a positive effect on wound and burn healing.[37] So excellent antibacterial properties can be achieved without compromising the original biological functions of the Ti through introducing the proper amount of Ag into the implants and controlling its release.[38]

There are many studies reporting that various techniques have been developed to obtain Ag nanoparticles decorated Ti-based implants. Particularly, the surface modification for Ag nanoparticles can be classified into three categories: (1) surface enrichment of Ag nanoparticles on the Ti-based implant while a layer is not introduced, (2) doping of Ag nanoparticles on the oxide layer (TiO_2) grew on the surface, and (3) doping of Ag nanoparticles on a coating (TiO_2 and foreign matter, e.g., hydroxyapatite) deposited on the surface.[39] In detail, Ag nanoparticles can be incorporated onto the Ti surfaces through ion implantation,[40] electrochemical techniques,[41] in situ preparation of Ag nanoparticles,[33] the sol−gel technique,[42] sputtering,[43] and so on.[44] Among these methods, in situ preparation of Ag nanoparticles has been proved to be a useful and simple way to modulate the amount of deposited nanoparticles and control the size of Ag nanoparticles on the surface.[39]

However, the biocompatibility of the Ti-based implants should not be ignored, especially the release of Ag^+ that we should pay attention to, as many works attributed the toxicity of Ag NPs to the Ag^+ release[45,46] and Ag^+ is very toxic to the human body.[18] Because of its nontoxicity and biodegradability, as a natural organic material, chitosan (CS) is usually employed to improve the bioactivity of biomaterials with a bioinert nature. In order to reduce the bioavailability and alleviate the toxicity of Ag^+, CS was introduced onto the Ti surface.

In this study, a nanostructured film composed of one-dimensional TNWs is employed as a carrier of Ag nanoparticles, and a CS nanofilm on the surface of Ag nanoparticles was fabricated. A TNWs film is produced on the Ti substrate by alkali hydrothermal reaction and subsequently doped by Ag nanoparticles through an ultraviolet light chemical reduction. The CS nanofilm was deposited on the Ag nanoparticles through spin-assisted layer by layer assembly methods. This course can be schematically illustrated by Scheme 1. Their antibacterial effect has also been studied. Finally, we have studied the influence of TNWs, and Ag and Ag/CS TNWs on the proliferation and differentiation of osteoblasts.

Scheme 1. Preparation Process Diagram of a TNWs/Ag/CS System on Ti Implants

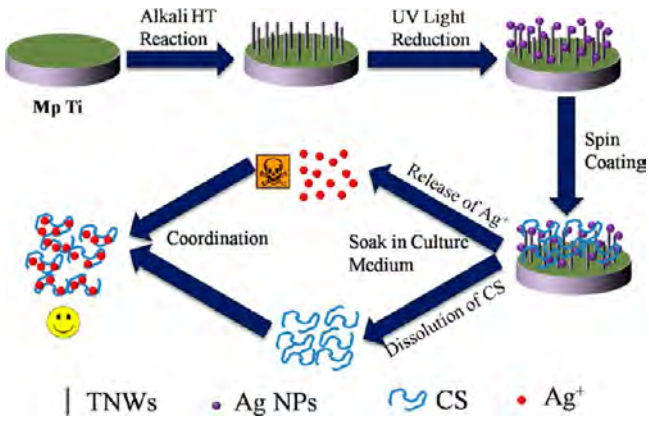

2. EXPERIMENTAL PROCEDURE

2.1. Materials. Medical pure titanium (MP-Ti) was purchased from Fu-Tai Metal Materials Co. (China). HCl, NaOH, NaCl, $NaHCO_3$, KCl, $K_2HPO_4{\cdot}3H_2O$, $MgCl_2{\cdot}6H_2O$, $CaCl_2$, Na_2SO_4, ethanol, methanol, and acetone were purchased from Sinopharm Chemical Reagent Co. (China). $AgNO_3$ was purchased from Shang-Hai fine chemical industry material institute (China). Peptone, yeast extract, and agar were purchased from Thermo Fisher Oxoid (UK). CS (visicosity: 100−200, 179.17 MW) were purchased from Sigma-Aldrich.

2.2. Preparation of samples. MP-Ti with dimension about 2 cm × 2 mm were employed as substrates. Prior to alkali-heat treatment, the Ti plates were successively polished to a mirror side by different grid abrasive paper and then they were ultrasonically rinsed in ethanol and deionized water successively.

Then the Ti plates were placed in a 100 mL Teflon-sealed autoclave containing 60 mL NaOH solution with different concentrations (0.2 mol/L, 0.5 mol/L, 1 mol/L, 2.5 mol/L). The vessel was hydrothermally treated at 180 °C for 72 h, and then cooled to room temperature in air. Then the samples was washed with deionized water, immersed in 0.05 mol/L HCl for 12 h and washed with deionized water to neutral conditions. These could be denoted as c-0.2, c-0.5, c-1, c-2.5, respectively.

The c-1 was immersed in $AgNO_3$ solution with different concentrations (0.01 mol/L, 0.02 mol/L). The samples were treated under ultrasonication for 30 min. Then the samples were immersed in 0.1 mol/L methanol and irradiated with 12 W UV-light (λ = 253 nm) for 40 min. Finally, the samples were washed with deionized water. These samples could be denoted as Ag-0.01 and Ag-0.02.

Methodology of spin-coating was used to prepare CS coating. Solutions of 2 mg/mL CS 1% (v/v) acetic acid were deposited onto the Ag-0.01 and Ag-0.02, followed by spinning at 800 rpm for 20 s to allow uniform spreading of the solution on the surface of substrates, then at 4000 rpm for 30 s to thin the solution layer, and finally dried in the air. Each sample repeats the spin process three times. These samples could be denoted as Ag/CS-0.01, Ag/CS-0.02.

2.3. Characterization. Scanning electronic microscopy (SEM) images were recorded on JSM-6510LV electron microscope (JEOL, JP). Transmission electron microscopy (TEM) images were recorded on a Tecnai G20 electron microscope (FEI, USA). Infrared (IR) spectroscopy was measured by NICOLET iS10 IR spectrophotometer (Nicolet, USA). X-ray diffraction (XRD) was recorded on D/Max-RB X-ray diffractomer (Rigaku, JP). Field emission scanning electron microscopy (FE-SEM) was recorded on JSM7100F (JEOL, JP). Inductive coupled plasma atomic emission spectrometry (ICP-AES) was carried out to determine the Ag release behaviors on an Optimal 8000 (PE, USA).

2.4. Contact angle. The contact angles of Ti plates were determined at room temperature by a contact angle instrument (OCA 40 Filderstadt, Germany). Deionized water was utilized as the medium

DOI: 10.1021/acsami.6b04161
ACS Appl. Mater. Interfaces 2016, 8, 16584−16594

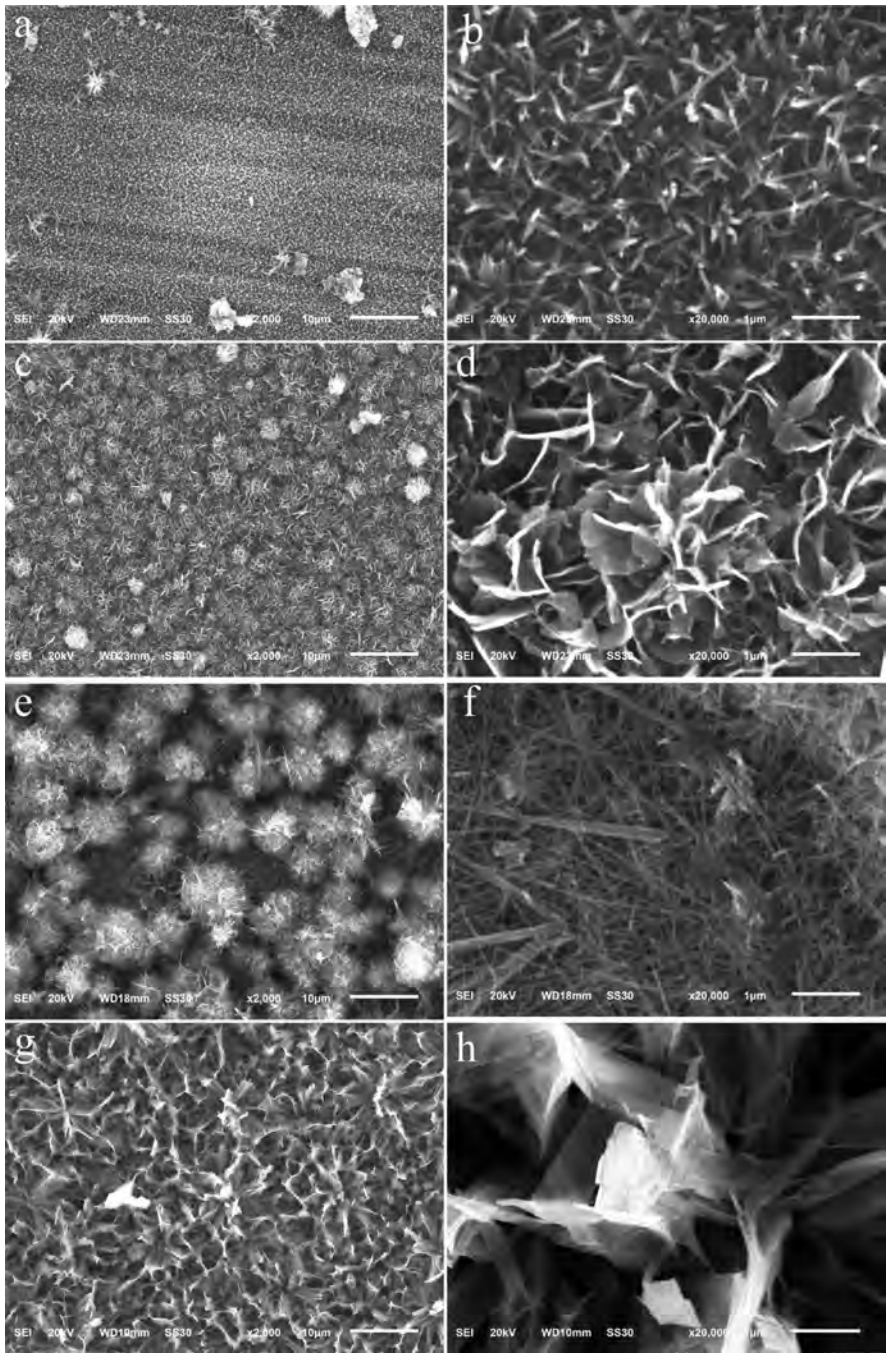

Figure 1. Surface morphologies of a Ti plate treated with different concentrations of NaOH. (a) 0.2 mol/L, (b) high-magnification of (a); (c) 0.5 mol/L, (d) high-magnification of (c); (e) 1 mol/L, (f) high-magnification of (e); (g) 2.5 mol/L, (h) high-magnification of (g).

to determine the contact angles. All the values are the average of 3 drops at 3 different positions on Ti plates surface.

2.5. *In vitro* bioactivity in simulated body fluid (SBF). The bioactivity of different Ti plates, in terms of apatite forming capability, was evaluated by soaking in SBF. The SBF was prepared according to standard ingredient.[15] All the Ti plates were immersed in SBF for 14 days at 37 °C.

2.6. Antibacterial study. *Escherichia coli* (*E. coli*) and *Staphylococcus aureus* (*S. aureus*) were employed to evaluate the antibacterial activity of the different Ti plates. They were cultured in standard Luria−Bertani (LB) culture medium. Sterile LB broth and LB agar plates were prepared in deionized water according to the standard procedure.[26]

LB agar plates seeded with bacteria were used to measure the zones of inhibition. The bacteria were diluted with melted LB agar plates to OD = 0.001. Then they were poured onto watch glass. All the Ti plates were lay on the surface of seeded LB agar plate and incubated at 37 °C for 12 h with *E. coli* and *S.aureus*.

Bacterial growth can be reflected by determining optical density (OD) at 600 nm of the culture medium. And bactericidal ratio can be applied to estimate the antibacterial activity of different Ti plates, which was determined by the following equation:[47]

$$\text{Bacterial ratio (\%)} = \frac{\text{OD of control group} - \text{OD of experimental group}}{\text{OD of control group}} \times 100\% \quad (1)$$

DOI: 10.1021/acsami.6b04161
ACS Appl. Mater. Interfaces 2016, 8, 16584−16594

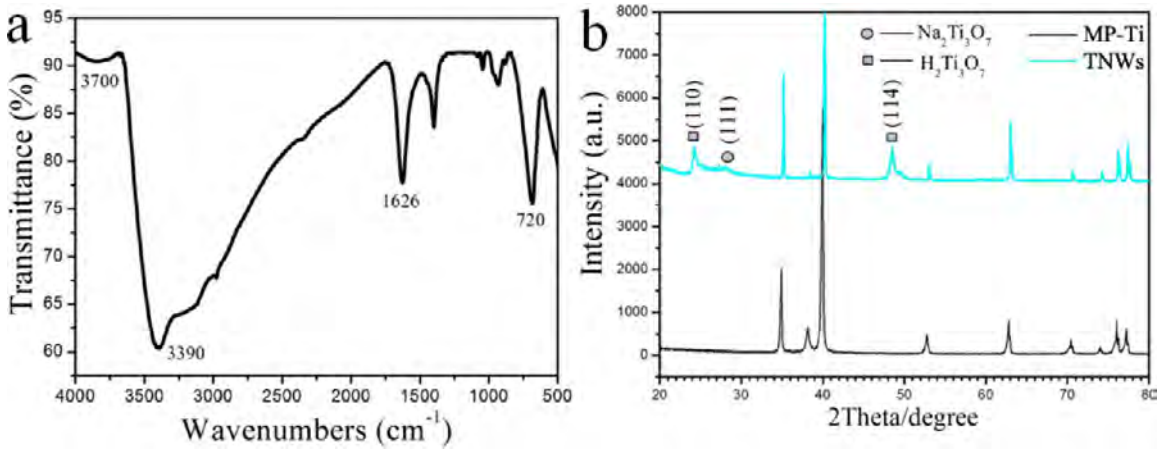

Figure 2. Surface composition and crystalline structures of TNWs. (a) IR spectra of the TNWs; (b) XRD spectra of the TNWs.

For the SEM observation, the bacterial suspension was incubated with the different Ti plates for 4h. Then the Ti plates were fixed with 2.5% glutaraldehyde (Sinopharm Chemical Reagent Co. China) for 4h, then they were dehydrated sequentially in a series of ethanol concentration gradient of 30, 50, 75, 90, 95, and 100 v/v %, and freeze-dried. The morphologies of bacteria on Ti plates were examined by SEM.

2.7. Cytotoxicity evaluation. *2.7.1. MTT assay.* The preosteoblast MC3T3 Cell of Mice was cultured by dulbecco's modified eagle medium (DMEM) supplemented with 10% fetal bovine serum, 1% penicillin and 1% amphotericin at 37 °C in 5% CO_2. The treated and untreated Ti plates were placed in 24-well plate. The cells were seeded into 24-well plate. After incubation for different periods (1 day, 3 days, 7 days), MTT (Aladdin Reagent Co., China) with a concentration of 0.5 mg/mL was added, the cells were allowed to incubated with MTT for 4 h until a purple precipitate was visible. The MTT solution was then removed and 150 μL DMSO was added to completely dissolve the crystals through vibrating for 10 min. Finally, the absorption at 490 nm was measured by Micropalte reader (SpectraMax I3MD USA).

2.7.2. Cell morphology. The cells were seeded onto the different Ti plates. After incubating for 24h, the seeded cells were rinsed with PBS (pH 7.4) three times and 4% formaldehyde (Sinopharm Chemical Reagent Co. China) solution in PBS (pH 7.4) was added to fix the cells for 10 min at room temperature, followed by rinsing with PBS three times. Then they were stained with FITC-phalloidin (YiSen, Shanghai) at room temperature for 30 min in the absence of light illuminated. Subsequently, they were rinsed with PBS for three times and further staining with DAPI (YiSen, Shanghai) for 30s. The cytoskeletal actin, and cell nuclei were observed by fluorescent microscopy (IX73, Olympus, USA).

2.7.3. Detection of intracellular ALP. The treated and untreated samples were placed in 24-well plate. The cells were seeded into 24 well-plate. After incubation for different periods (3 days, 7 days, 14 days), the cells were lysed in 1% Triton X-100 (Sinopharm Chemical Reagent Co. China) dissolved in PBS and stored in 4 °C for 30 min. Then they were centrifuged (1100 rpm/min) for 10 min and 10 μL supernatant was transferred into 96-well plate. Finally, the intracellular ALP activity was detected by ALP detection kit (Jiancheng Biotech, China).

3. RESULTS AND DISCUSSIONS

3.1. Characterization of Ti plate after hydrothermal treatment (HT Ti). *3.1.1. Micromorphology.* After hydrothermal treatment, the Ti plates display different micromorphology. As shown in Figure 1, a lower concentration of NaOH induces a small needle-like microstructure on the surface of the Ti plate, which is uniformly distributed on the whole surface (c-0.2, Figures 1a and 1b). As the NaOH concentration increases to 0.5 mol/L, flower-like nanoclusters are formed on the entire surface (c-0.5, Figure 1c), and each cluster is composed of petal-like nanosheets (c-0.5, Figure 1d). In addition, when the NaOH concentration increases to 1 mol/L, clusters of dandelion-like microstructure appear on the whole surfaces (Figure 1e). It can be observed from the high resolution image (Figure 1f) that these dandelion-like microstructures consist of crossed nanowires. Compared with c-0.2, the aspect ratio of c-1 is much larger. As the concentration of NaOH increased to 2.5 mol/L, the surface is covered with a sheet-like structure (Figure 1g), and the sheet size is very large and seems like a band or bulk material (Figure 1h).

3.1.2. Composition of TNWs. IR was employed to study the surface composition of TNWs on the Ti substrate. As shown in Figure 2a, the absorption peak at 3390 cm^{-1} can be assigned to the stretching vibrations of O−H, which indicates that Ti−OH exists on the surface of TNWs. And the peaks at 3700 and 1626 cm^{-1} can be attributed to the stretching vibrations and bending vibration of O−H in hydrate water, respectively. The peak at 1400 cm^{-1} may stem from the stretching vibration of the Ti−O−Ti. In addition, the peak for the stretching vibration of the Ti−OH at 925 cm^{-1} is observed. The elemental composition of TNWs was analyzed by X-ray energy dispersion spectroscopy (EDS). The EDS spectrum of TNWs is shown in Figure S1; the results disclose that the surface of TNWs is composed of Ti, O, and Na (Figure S1). So the surface of TNWs is converted to titanate after hydrothermal treatment and hydrate water also exists on the surface of TNWs ($Na_yH_{2-y}TinO_{2n-2}\cdot xH_2O$).

The crystal structures of the prepared TNWs were characterized by XRD. The diffraction peaks at 24.2° and 48.5° can be assigned to (110) and (114) of $H_2Ti_3O_7$, while the peak centered between 23°−25° is associated with (111) of $Na_2Ti_3O_7$ (Figure 2b). The XRD spectra further prove that both $H_2Ti_3O_7$ and $Na_2Ti_3O_7$ exist in the nanofilm on the Ti substrates. The reason for the much weaker diffraction intensity of $Na_2Ti_3O_7$ may be due to the fact that the HT Ti plate has been immersed into diluted HCl for 12 h. So the surface of TNWs was functionalized with Ti−OH, which could attract the Ca^{2+} and then PO_4^{3-} to form the bone-like apatite layer. In a word, a nanostructured film composed of one-dimensional TNWs can be successfully fabricated through this method.

3.1.3. Wettability of the HT Ti. The degree of surface wettability of the desired materials is characterized by contact angle analysis. The value of the contact angle can be employed as an indicator of the surface wettability of the material when employed as a biomedical implant.

DOI: 10.1021/acsami.6b04161
ACS Appl. Mater. Interfaces 2016, 8, 16584−16594

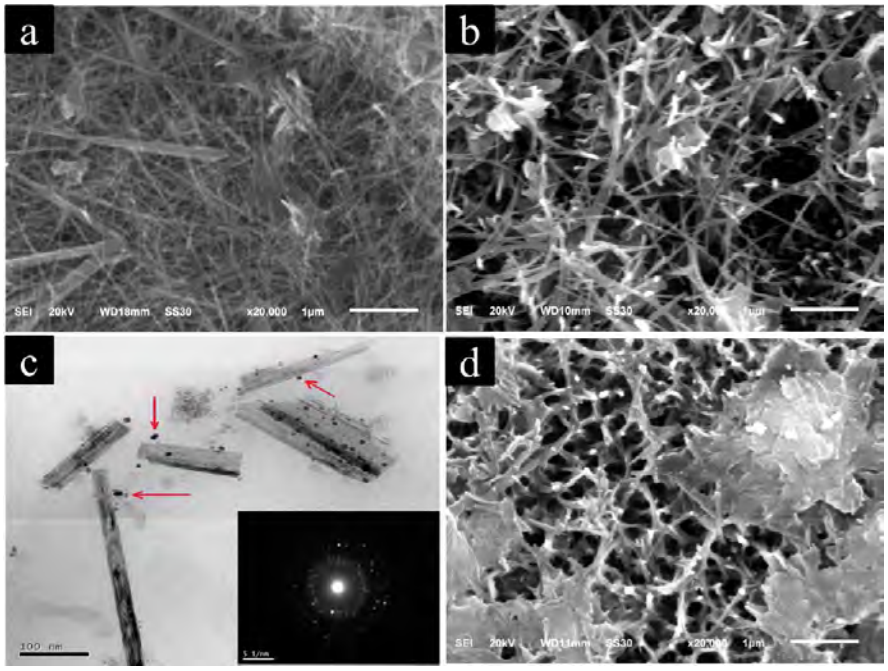

Figure 3. Surface morphologies of undoped, Ag doped, and Ag/CS capped TNWs. (a) SEM images of undoped TNWs; (b) SEM images of Ag doped TNWs; (c) TEM images of Ag doped TNWs (Inset: SAED pattern of Ag nanoparticles); (d) SEM images of Ag/CS capped TNWs.

Figure 4. Images of water droplets lying on flat Ag doped and Ag/CS capped TNWs.

Images of water droplets lying on HT Ti surfaces are shown in Figure S2. And the corresponding contact angle values are listed in Table S1. Deionized water dropped on an MP Ti plate shows an angle of 63.3°, which indicates some amount of hydrophobicity. As shown in Figure S2, the contact angle is decreased significantly as the concentration of NaOH increased. When the concentration is up to 2.5 mol/L, drops of water spread out rapidly on the surface of Ti plates and the contact angle is close to 0°.

Our measured results on MP Ti were in agreement with other reports.[15] The improvement of the surface wettability for HT Ti may partially stem from the gradual increase of the oxygen content. When the NaOH solution reaches 2.5 mol/L, the values of the contact angles turn to 0°, i.e., superhydrophilicity. However, in this case, the morphology of the nanostructures should also not be underestimated. In addition, it is very clear that the one-dimensional TNWs also display superhydrophilicity.

The surface hydrophilicity affects the biological functions of biomaterials such as bacteria/cell adhesion and spreading. Several works have reported that fibroblast cells like to attach and spread on the hydrophilic surface compared with the hydrophobic surface.[48] However, unlike the case of a fibroblast, a superhydrophilic surface favors the attachment of osteoblasts.[49] So the prepared samples with better wettability favor the formation of the tissue fragments and are easier to incorporate with the surrounding biological environment.[50]

3.2. Characterization of Ag doped and Ag/CS capped TNWs. *3.2.1. Micromorphology.* First, SEM and TEM were used to study the micromorphology of a Ag doped TNWs coating. As shown in the SEM images (Figure 3), compared with undoped samples (Figure 3a), many white small dots are attached to the TNWs (Figure 3b). In addition, as shown in the TEM images (Figure 3c), TNWs are attached by small black dots while these black dots cannot be observed in the undoped samples. In addition, the SAED pattern (inset of Figure 3c) of Ag nanoparticles prepared by UV light chemical reduction showed several diffraction rings, which stem from the random orientation of the crystal. This suggested that the sample was nanocrystalline in nature. So these black dots distributed uniformly on the TNWs are speculated to be Ag nanoparticles, and their sizes are between 3 and 5 nm. The morphology of Ag/CS capped TNWs is shown in Figure 3d, it is obvious that a thin layer of nanofilm made up of CS molecules is deposited on the surface of TNWs. Ag nanoparticles identified by white small dots can also be observed in the images. The existence of Ag could be further identified by the EDS spectra.

3.2.2. Composition and structure analysis. The elemental analysis is carried out by EDS. The EDS spectra of Ag doped samples are shown in Figure S3a. The Ag doped TNWs consist of Ti, Ag, Na, and O. The content of Ti derived from the substrate is the highest while the signal of Ag element is also intensive, indicating that the Ag is doped onto TNWs successfully. In addition, as shown in Figure S3b, the Ag/CS capped TNWs contain Ti, Ag, N, Na, and O. The content of Ag in Ag/CS capped TNWs is smaller than that of Ag doped TNWs.

The XRD spectra of doped and undoped TNWs are given in Figure S4. Compared with undoped samples, extra peaks (2θ = 44.96°) are observed in the Ag doped and Ag/CS capped TNWs. This characteristic diffraction peak is consistent with the peak of metallic Ag. The peaks at 45.59° can be assigned to

DOI: 10.1021/acsami.6b04161
ACS Appl. Mater. Interfaces 2016, 8, 16584−16594

(104) of metallic Ag. So it is very clear that the Ag was doped onto the TNWs successfully in this work.

3.2.3. Wettability of the Ag doped and Ag/CS capped TNWs. The wettabilities of the Ag doped and Ag/CS capped TNWs have also been studied. Images of water droplets and the corresponding values of the contact angle are exhibited in Figure 4 and Table 1, respectively. As shown in Figure 4, in comparison with TNWs modified Ti plates (Figure S2), the contact angles increase obviously for Ag/TNWs modified Ti, which indicates that the Ag doping on TNWs can change the surface hydrophilicity of TNWs modified Ti. Interestingly, when the CS nanofilm was deposited on the Ag nanoparticles, the contact angle decreased significantly close to nearly 0°, enhancing the superhydrophilicity of the modified surface, which is possibly ascribed to the superior hydrophilicity of the CS molecule. Since surface hydrophilicity favors the adhesion of osteoblasts on biomaterials,[49] the CS capped Ag/TNWs with better wettability will benefit the bone cell growth on Ti plates and consequently be conducive for the osteointegration of implants within the surrounding biological system.[50]

Table 1. Contact Angle Values of Ag Doped and Ag/CS Capped TNWs

	Ag-0.01	Ag-0.02	Ag/CS-0.01	Ag/CS-0.02
Angles (deg)	54	53	13	16

3.2.4. In vitro bioactivity. The SEM images of Ag doped and Ag/CS capped TNWs before and after soaking in SBF for 14 days are displayed in Figure 5. A rod apatite-like structure is observed on the Ag doped TNWs (Figure 5c), and spherical globules are formed on Ag/CS capped TNWs (Figure 5d). However, the area of the apatite-like structure on the Ag/CS capped TNWs is much larger than that of Ag doped TNWs. This can be further verified by the EDS spectra (Figure S5). According to EDS analysis, the Ca/P ratios of two TNWs for the agglomerates are basically close to the theoretical ratio of Ca/P in hydroxyapatite. However, the content of Ca in Ag/CS capped TNWs is slightly larger than that in Ag doped TNWs. So the Ag/CS capped TNWs are more beneficial to the deposition of Ca−P, which is in good agreement with wettability results.

It is well accepted that if the surfaces of biomaterials can be helpful for the formation of hydroxyapatite on surfaces in SBF; they are beneficial for the formation of new bone tissues *in vivo* as well as accelerating the bone integration.[15] As the ingredient of this apatite layer is similar to the mineral phase in bone, so it can be recognized by the living body.[51]

3.3. Antibacterial study. During the course of surgery, metallic orthopedic implants very easily suffer bacterial infections, which may cause serious microbial attack and the subsequent final failure of the implants. Some antimicrobial strategies have been developed to overcome bacterial infection. In this work, an antibacterial agent (Ag nanoparticles) can be doped into the TNWs by UV light chemical reduction to study the antibacterial activity of the implant. Moreover, an antibacterial and biocompatible polymer (CS) is deposited on the coatings to improve the antibacterial activity and biocompatibility of the implants.

The Ag doped and Ag/CS capped TNWs show strong antibacterial activities against both *E. coli* and *S. aureus*. Figure 6 shows the antibacterial activity of MP Ti, TNWs, and Ag doped and Ag/CS capped TNW coatings against *E. coli* and *S. aureus*. As shown in Figure 6, an MP Ti plate does not show any antibacterial activity. The MP Ti plates are attached by the *E. coli* cells, and the whole Petri dish is covered with *E. coli*. In addition, an undoped TNW sample also does not show any antibacterial activity. However, Ag doped and Ag/CS capped TNWs show a clear bacterial inhibition zone to *E. coli* and *S. aureus*. The sizes of the inhibition zone increase with the

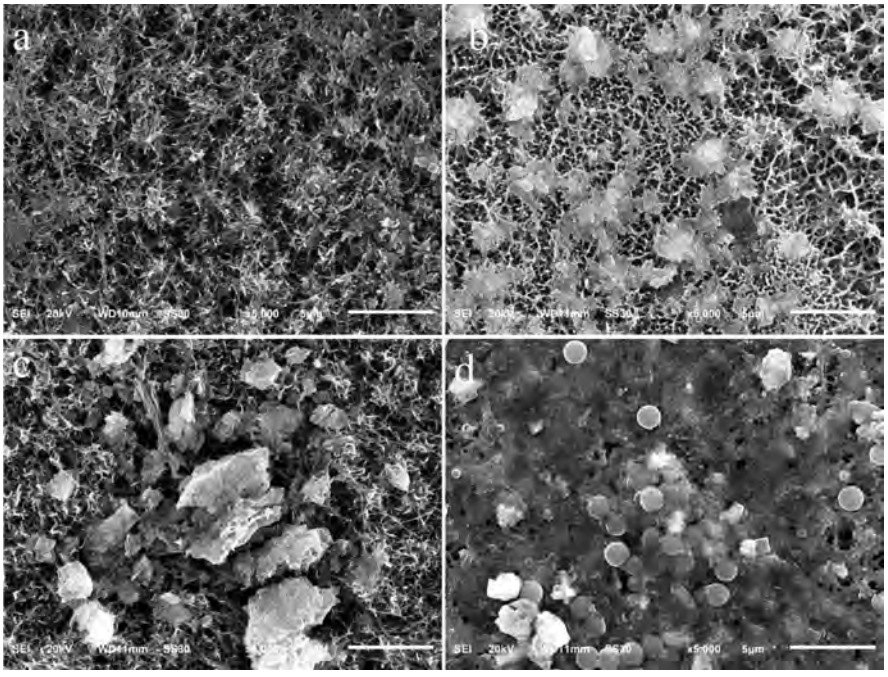

Figure 5. Surface morphologies of Ag doped and Ag/CS capped TNWs before and after soaking in SBF for 14 days. SEM images of Ag doped TNWs before (a) and after (c) soaking in SBF for 14 days. SEM images of Ag/CS capped TNWs before (b) and after (d) soaking in SBF for 14 days.

DOI: 10.1021/acsami.6b04161
ACS Appl. Mater. Interfaces 2016, 8, 16584−16594

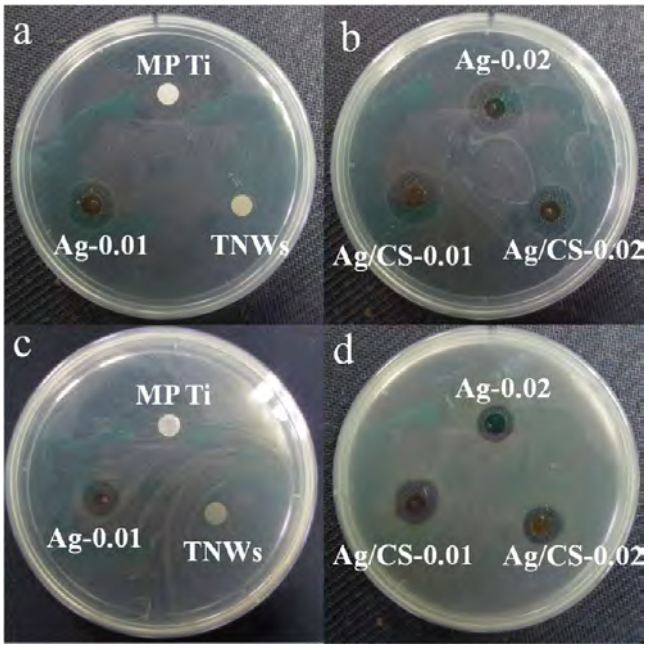

Figure 6. Disk diffusion test for MP Ti, TNWs, and Ag doped and Ag/CS capped TNWs against *E. coli* (a and b) and *S. aureus* (c and d).

increase of Ag content. Interestingly, the inhibition zone sizes of Ag/CS capped TNWs are larger than that of Ag doped TNWs.

Bacterial growth can also be reflected by the change of OD at 600 nm. Quantitative analysis also indicates that both Ag doped and Ag/CS capped TNWs exhibit strong antibacterial activities against both *E. coli* and *S. aureus* (Figure 7a). The antibacterial activities increase with the increase of Ag content, and CS can also improve the antibacterial effect of the hybrid coatings.

The morphologies of bacteria attached on the Ti surface are examined by SEM. As shown in Figure S6, *E. coli* and *S. aureus* display regular morphology and intact surface on MP Ti substrates after 4 h of incubation. And both the bacteria would not attach to the surface of TNWs. However, the bacteria obviously exhibit impaired structure on Ag doped TNWs and Ag/CS capped TNWs. *E. coli* on Ag doped TNWs and Ag/CS capped TNWs lose their smooth and long-chain structures, and cell membranes begin to fester, which indicate that these bacteria are inactivated. Likewise, *S. aureus* on Ag doped TNWs and Ag/CS capped TNWs exhibit a shrinkage cell membrane shape from a round smooth shape. In a word, Ag doped and Ag/CS capped TNWs can display an obvious negative effect on the morphologies of *E. coli* and *S. aureus*.

These results indicated that Ag TNWs actually had an antibacterial effect and CS capped on TNWs could further increase the antibacterial activity of TNWs. These coatings could display broad-spectrum antibacterial properties against *S. aureus* (Gram-positive) and *E. coli* (Gram-negative).

3.4. Ag release. The antibacterial activity of Ag nanoparticles derived from the release of Ag^+ from the nanoparticles. The Ag^+ is more easily released from Ag nanoparticles when immersed in a practical biological system, such as practical body fluid.[46]

The Ag doped samples were separately immersed in a SBF solution, mimicking human body conditions, and the content of leached Ag was determined by ICP-AES. The released Ag^+ possesses high activity, and it can endow a deleterious effect on multiple sites within bacteria. For example, Ag^+ could interact with nucleic acids and DNA molecules became condensed and lost their replication ability after treatment with Ag^+.[52] Another study reported that Ag^+ could also inhibit respiratory enzymes, accelerate the production of reactive oxygen species (ROS), and interfere with the membrane permeability, consequently leading to bacterial death.[18]

The influence of immersion time on the content of Ag^+ released in SBF is shown in Figure 7b. The release rate of Ag doped TNWs is very fast in the first 5 days, and the rate gradually slows down in the following days. So continuous Ag^+ released from the coatings can be realized for the Ag/TNWs modified Ti implants. In addition, as the content of $AgNO_3$ is increasing in the initial UV light reduction system, the Ag content released from the materials obviously increases. The release behavior of Ag^+ from TNWs displays the same trend

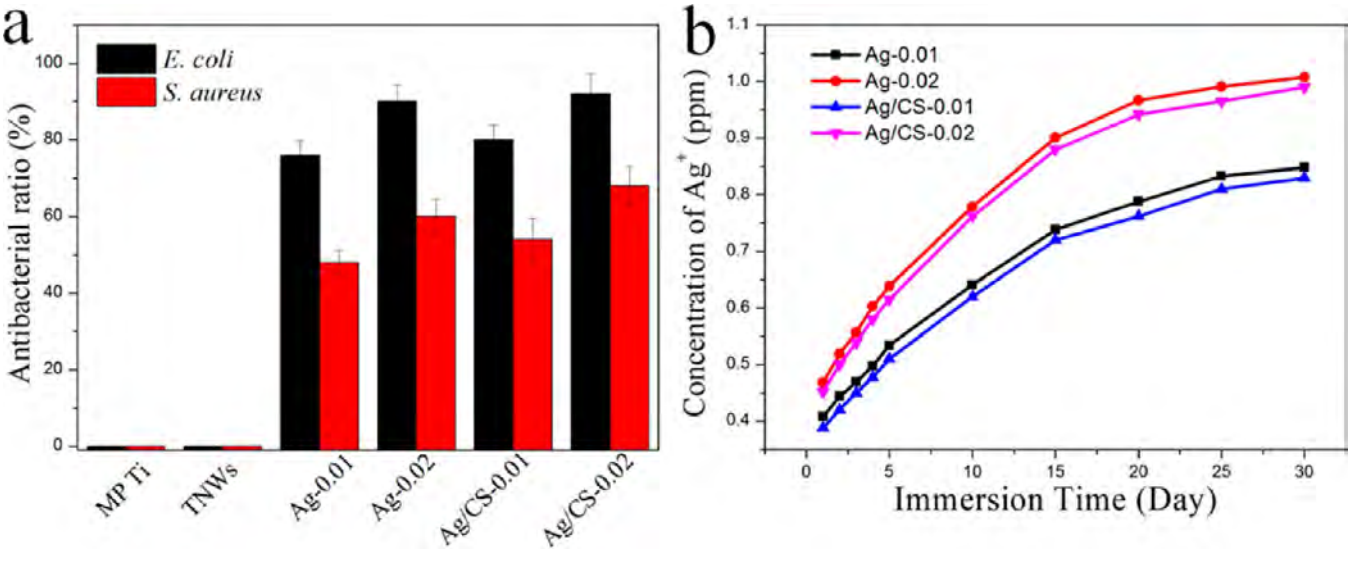

Figure 7. (a) *In vitro E. coli* and *S. aureus* antibacterial activity of different coatings (mean ± SD, $n = 3$). (b) Ag^+ release from Ag doped and Ag/CS capped TNWs in SBF.

DOI: 10.1021/acsami.6b04161
ACS Appl. Mater. Interfaces 2016, 8, 16584−16594

while the corresponding Ag^+ concentration is a little smaller than that of Ag doped TNWs.

The mechanism for Ag^+ release can be studied by fitting the releasing curves through classic drug releasing models. Then the releasing curves presented in Figure 7b are fitted by a simple Peppas model (eq 2):[53]

$$Q = kt^n \quad (2)$$

where Q represents the proportion of total Ag^+ released from the Ag nanoparticles. The kinetic constant and releasing exponent can be denoted by k and n, respectively. The values of n can be employed to illustrate the mechanism of Ag^+ release. As for the thin film model, when $n < 0.5$, Fickian type release dominates, while if $0.5 < n < 1$, the release is non-Fickian type. When the releasing mechanism is zero order type, the releasing exponent is equal to 1. The values of n of the Ag releasing curves are listed in Table 2. They are all less than 0.5, which indicates that Ag^+ release is dominated by Fickian type.

Table 2. Ag Release Kinetics Parameters Obtained from the Peppas Model

Sample	k	n	R^2
Ag-0.01	0.435	0.248	0.985
Ag-0.02	0.433	0.255	0.988
Ag/CS-0.01	0.421	0.258	0.989
Ag/CS-0.02	0.423	0.261	0.986

So it is very clear that the initial concentrations of released antimicrobial agents (Ag^+) from Ag doped and Ag/CS capped TNWs is very high. As the implants very easily suffer from the adhesion of bacteria after the implantation surgery, this releasing behavior can prevent bacterial adhesion.[54] Moreover, long-term and sustained release of Ag^+ after implantation surgery is also very essential to prevent bacterial biofilm formation on Ti-based metallic implants.

3.5. Biocompatibility of TNWs. The cytotoxicity of MP Ti plates, TNWs, and Ag doped and Ag/CS capped TNWs was determined by MTT assay against preosteoblast MC3T3 cells of mice (Figure 8a). The effects of Ti plate and HT Ti on the proliferation rate of MC3T3 cells are shown in Figure 8a. When the cells were cultured with samples, the cell viability of cells cultured on TNWs was comparable with the MP Ti. However, the Ag doped TNWs were toxic to MC3T3-E1 and the cell viability was close to 0. Interestingly, the Ag/CS capped TNWs increased the cell viability obviously. In addition, with the increasing of culture time, the cell viability of MC3T3 on Ag/CS capped TNWs increased obviously. When the cells were cultured with samples for 7 days, the cell viability reached 68% and 54% for Ag/CS-0.01 and Ag/CS-0.02 TNWs, respectively.

There was an interesting phenomenon needed to be paid attention to, namely, when the Ag doped and Ag/CS capped TNWs were immersed in SBF for 7 days, the released Ag^+ showed a much higher concentration than that of TNWs immersed in SBF for 1 day. Nevertheless, when the incubation time increased from 1 to 7 days, the cell viability of MC3T3 obviously increased (Figure 8a). Xiu et al. have assigned the toxicity of Ag NPs to the Ag^+ release alone, and morphologies of Ag NPs affect their antibacterial properties, primarily through affecting release of Ag^+.[46] Moreover, the bioavailability and toxicity of Ag^+ can be reduced via binding of ligands in the medium to the Ag^+.[55] CS $(C_6H_{11}NO_4)_n$ can be used as an effectient absorbent to remove the metal ions from the environment or living body. The polymer chains of CS are functionalized with abundant amino and hydroxyl which can be employed as binding sites for metal ions.[56] The molecular structure and coordination process of CS to Ag^+ have been shown in Figure S7. So we speculate that CS nanofilms on the TNWs can partially dissolve into the culture medium and the release rate of CS is lower than that of Ag^+. Then the CS can bind to the Ag^+ via coordination and the bioavailability of Ag^+ obviously reduces. Finally, the toxicity of Ag^+ is hindered, which contributed to the increase of cell viability for 7 days. So the biocompatibility of metallic implants could be controlled by modulating the bioavailability of released Ag^+.

The initial cell adhesion and spreading activity of MC3T3 seeded on the samples is studied by fluorescence microscopy. Cell nuclei and cytoplasmic actin skeletons are visualized under fluorescence microscopy through DAPI and FITC-phalloidin staining, respectively. As shown in Figure S8, the cell can adhere and spread on the TNWs and Ag/CS capped TNWs. However, the fluorescent micrographs show that the cells cannot adhere on the Ag doped TNWs, which is in accordance with the MTT assay (data not shown). Furthermore, the

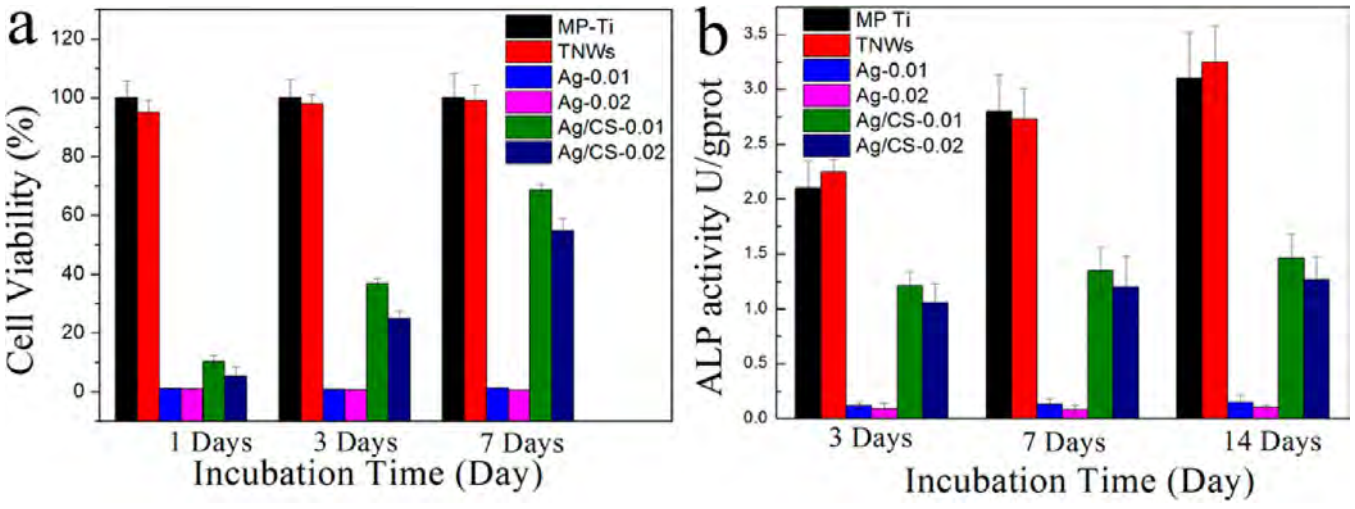

Figure 8. Effects of various coatings on the cell viability (a) and ALP activity (b) of preosteoblast MC3T3 cells of mice (mean ± SD, $n = 3$).

DOI: 10.1021/acsami.6b04161
ACS Appl. Mater. Interfaces 2016, 8, 16584−16594

relative number of cells adhered on the Ag/CS capped TNWs is smaller than that on the TNWs. Moreover, the cell morphology on the TNWs is more regular than that on the Ag/CS TNWs. Several cells with irregular spherical morphology are observed in the Ag/CS TNWs. In addition, more filopodia is observed in the cells on TNWs, which illustrates the better spreading activity of osteoblasts. All these results are in great accordance with the MTT assay.

ALP activity is usually utilized as an indicator to evaluate the early differentiation level of osteoblast cells, as it is an signficant element to promote the formation of bone tissues at the surface of implants.[57] As illustrated in Figure 8b, the normalizd ALP activity for the most samples increased from 3 and 14 days. When the cells were cultured on Ag doped TNWs, the ALP activity was very low. Interestingly, the Ag/CS capped TNWs coatings obviously increased the ALP activity of the cells. Comparison of the aforementioned *in vitro* results suggested that the addition of CS could reduce the toxicity of Ag nanoparticles in the coatings.

4. CONCLUSIONS

The NaOH concentration of hydrothermal treatment has a great influence on the micromorphology of HT Ti plates. When the concentration of NaOH was set as 1 mol/L, a nanostructured film composed of one-dimensional titanate nanowires (TNWs) was successfully obtained. Compared with an untreated Ti plate, the wettability of TNWs modified Ti is obviously improved. The metallic Ag can be incorporated into HT Ti plates through a UV light reduction method. The Ag nanoparticles with sizes between 3 and 5 nm distributed uniformly on the TNWs. This Ag doped into the TNWs actually has an antibacterial effect, and this effect increases with the improvement of Ag dose. The CS nanofilm improves the antibacterial activity of the TNWs. Both Ag doped and Ag/CS capped TNWs can provide high initial concentration and the continuous release of antimicrobial agent in surrounding biological environments. Although the Ag doped TNWs are toxic to the cells, the CS nanofilm can obviously improve the biocompatibility of Ag/TNWs, which is very meaningful for the clinical application of metallic implants.

■ ASSOCIATED CONTENT

Supporting Information

The Supporting Information is available free of charge on the ACS Publications website at DOI: 10.1021/acsami.6b04161.

Contact angle values of prepared HT Ti; EDS spectrum of TNWs; images of water droplets lying on flat prepared samples surfaces; EDS spectra of Ag doped and Ag/CS capped TNWs; XRD spectra of Ag doped and Ag/CS capped TNWs; EDS spectra of Ag doped TNWs and Ag/CS capped TNWs soaked in SBF for 14 days; morphologies of *E. coli* and *S. aureus* attached on the MP Ti, Ag doped TNWs and Ag/CS capped TNWs; molecular structure of CS and scheme for coordination process of CS to Ag^+; fluorescent images of MC3T3 cells cultured on TNWs and Ag/CS TNWs for 24 h (PDF)

■ AUTHOR INFORMATION

Corresponding Authors

*E-mail: shuilin.wu@gmail.com. Tel: +86-27-88661729. Fax: +86-27-88665610 (S. L. Wu).

*E-mail: yonghan@mail.xjtu.edu.cn (Y. Han).

Author Contributions

⊥Z.X. and M.L. contributed equally.

Notes

The authors declare no competing financial interest.

■ ACKNOWLEDGMENTS

This study was jointly supported by the Special Prophase Program for Key Basic Research of the Ministry of Science and Technology of China (973 Program), grant no. 2014CB660809; the National Natural Science Foundation of China, grant nos. 51422102 and 81271715; the Hong Kong Research Grants Council (RGC) General Research Funds (GRF) No. 112212 and 11301215, Hubei Provincial Natural Science Foundation, grant nos. 2013CFA018 and 2014CFB551, as well as State Key Laboratory for Mechanical Behavior of Materials.

■ REFERENCES

(1) Niinomi, M. *Metals for Biomedical Devices*; Elsevier: 2010.

(2) Bordji, K.; Jouzeau, J.; Mainard, D.; Payan, E.; Netter, P.; Rie, K.; Stucky, T.; Hage-Ali, M. Cytocompatibility of Ti-6Al-4V and Ti-5Al-2.5 Fe Alloys According to Three Surface Treatments, using Human Fibroblasts and Osteoblasts. *Biomaterials* **1996**, *17*, 929−940.

(3) Pattanayak, D. K.; Fukuda, A.; Matsushita, T.; Takemoto, M.; Fujibayashi, S.; Sasaki, K.; Nishida, N.; Nakamura, T.; Kokubo, T. Bioactive Ti Metal Analogous to Human Cancellous Bone: Fabrication by Selective Laser Melting and Chemical treatments. *Acta Biomater.* **2011**, *7*, 1398−1406.

(4) Liu, X.; Chu, P. K.; Ding, C. Surface Modification of Titanium, Titanium alloys, and Related Materials for Biomedical Applications. *Mater. Sci. Eng., R* **2004**, *47*, 49−121.

(5) Wu, S.; Liu, X.; Yeung, K. W.; Liu, C.; Yang, X. Biomimetic Porous Scaffolds for Bone Tissue Engineering. *Mater. Sci. Eng., R* **2014**, *80*, 1−36.

(6) Dong, W.; Zhang, T.; Epstein, J.; Cooney, L.; Wang, H.; Li, Y.; Jiang, Y.-B.; Cogbill, A.; Varadan, V.; Tian, Z. R. Multifunctional Nanowire Bioscaffolds on Titanium. *Chem. Mater.* **2007**, *19*, 4454−4459.

(7) Jämting, Å.; Bell, J.; Swain, M.; Wielunski, L.; Clissold, R. Measurement of the Micro Mechanical Properties of sol-gel TiO_2 films. *Thin Solid Films* **1998**, *332*, 189−194.

(8) Uhm, S.-H.; Song, D.-H.; Kwon, J.-S.; Im, S.-Y.; Han, J.-G.; Kim, K.-N. Time-Dependent Growth of TiO_2 Nanotubes From a Magnetron Sputtered Ti Thin Film. *Thin Solid Films* **2013**, *547*, 181−187.

(9) Chen, H.-W.; Huang, K.-C.; Hsu, C.-Y.; Lin, C.-Y.; Chen, J.-G.; Lee, C.-P.; Lin, L.-Y.; Vittal, R.; Ho, K.-C. Electrophoretic Deposition of TiO_2 Film on Titanium Foil for a Flexible Dye-Sensitized Solar Cell. *Electrochim. Acta* **2011**, *56*, 7991−7998.

(10) Li, J.; Wang, G.; Geng, H.; Zhu, H.; Zhang, M.; Di, Z.; Liu, X.; Chu, P. K.; Wang, X. CVD Growth of Graphene on NiTi Alloy for Enhanced Biological Activity. *ACS Appl. Mater. Interfaces* **2015**, *7*, 19876−19881.

(11) Li, S.; Zhang, G.; Guo, D.; Yu, L.; Zhang, W. Anodization Fabrication of Highly Ordered TiO_2 nanotubes. *J. Phys. Chem. C* **2009**, *113*, 12759−12765.

(12) Wu, S.; Liu, X.; Hu, T.; Chu, P. K.; Ho, J.; Chan, Y.; Yeung, K.; Chu, C.; Hung, T.; Huo, K. A Biomimetic Hierarchical Scaffold: Natural Growth of Nanotitanates on Three-Dimensional Microporous Ti-based Metals. *Nano Lett.* **2008**, *8*, 3803−3808.

(13) Guo, Y.; Lee, N.-H.; Oh, H.-J.; Yoon, C.-R.; Park, K.-S.; Lee, H.-G.; Lee, K.-S.; Kim, S.-J. Structure-Tunable Synthesis of Titanate Nanotube Thin Films via a Simple Hydrothermal Process. *Nanotechnology* **2007**, *18*, 295608.

(14) Lai, Y.; Tang, Y.; Huang, J.; Wang, H.; Li, H.; Gong, D.; Ji, X.; Gong, J.; Lin, C.; Sun, L. Multi-Functional Hybrid Protonated Titanate Nanobelts with Tunable Wettability. *Soft Matter* **2011**, *7*, 6313−6319.

DOI: 10.1021/acsami.6b04161
ACS Appl. Mater. Interfaces 2016, 8, 16584−16594

(15) Wang, H.; Lai, Y.-K.; Zheng, R.-Y.; Bian, Y.; Zhang, K.-Q.; Lin, C.-J. Tuning the Surface Microstructure of Titanate Coatings on Titanium Implants for Enhancing Bioactivity of Implants. *Int. J. Nanomed.* **2015**, *10*, 3887−3896.
(16) Zhang, L.; Chen, Y.; Rodriguez, J.; Fenniri, H.; Webster, T. J. Biomimetic Helical Rosette Nanotubes and Nanocrystalline Hydroxyapatite Coatings on Titanium for Improving Orthopedic Implants. *Int. J. Nanomed.* **2008**, *3*, 323−333.
(17) Prabu, V.; Karthick, P.; Rajendran, A.; Duraipandy, N.; Kiran, M.; Pattanayak, D. K. Bioactive Ti Alloy with Hydrophilicity, Antibacterial Activity and Cytocompatibility. *RSC Adv.* **2015**, *5*, 50767−50777.
(18) Zhang, L.; Ning, C.; Zhou, T.; Liu, X.; Yeung, K. W.; Zhang, T.; Xu, Z.; Wang, X.; Wu, S.; Chu, P. K. Polymeric Nanoarchitectures on Ti-based Implants for Antibacterial Applications. *ACS Appl. Mater. Interfaces* **2014**, *6*, 17323−17345.
(19) Harris, L.; Tosatti, S.; Wieland, M.; Textor, M.; Richards, R. Staphylococcus Aureus Adhesion to Titanium Oxide Surfaces Coated with Non-functionalized and Peptide-Functionalized Poly (L-lysine)-Grafted-Poly (ethylene glycol) Copolymers. *Biomaterials* **2004**, *25*, 4135−4148.
(20) Zhao, L.; Chu, P. K.; Zhang, Y.; Wu, Z. Antibacterial Coatings on Titanium Implants. *J. Biomed. Mater. Res., Part B* **2009**, *91*, 470−480.
(21) Goodman, S. B.; Yao, Z.; Keeney, M.; Yang, F. The Future of Biologic Coatings for Orthopaedic Implants. *Biomaterials* **2013**, *34*, 3174−3183.
(22) Edupuganti, O. P.; Antoci, V.; King, S. B.; Jose, B.; Adams, C. S.; Parvizi, J.; Shapiro, I. M.; Zeiger, A. R.; Hickok, N. J.; Wickstrom, E. Covalent Bonding of Vancomycin to Ti6Al4V Alloy Pins Provides Long-Term Inhibition of Staphylococcus Aureus Colonization. *Bioorg. Med. Chem. Lett.* **2007**, *17*, 2692−2696.
(23) Jose, B.; Antoci, V.; Zeiger, A. R.; Wickstrom, E.; Hickok, N. J. Vancomycin Covalently Bonded to Titanium Beads kills Staphylococcus Aureus. *Chem. Biol.* **2005**, *12*, 1041−1048.
(24) Wang, Z.; Sun, Y.; Wang, D.; Liu, H.; Boughton, R. I. In situ Fabrication of Silver Nanoparticle-filled Hydrogen Titanate Nanotube Layer on Metallic Titanium Surface for Bacteriostatic and Biocompatible Implantation. *Int. J. Nanomed.* **2013**, *8*, 2903.
(25) Rajendran, A.; Vinoth, G.; Shanthi, V.; Barik, R.; Pattanayak, D. Silver Nano particle Incorporated Ti Metal Prepared by Chemical Treatment for Antibacterial and Corrosion Resistance Study. *Mater. Technol.* **2014**, *29*, B26−B34.
(26) Mei, S.; Wang, H.; Wang, W.; Tong, L.; Pan, H.; Ruan, C.; Ma, Q.; Liu, M.; Yang, H.; Zhang, L. Antibacterial Effects and Biocompatibility of Titanium Surfaces with Graded Silver Incorporation in Titania Nanotubes. *Biomaterials* **2014**, *35*, 4255−4265.
(27) Patel, J. S.; Patel, S. V.; Talpada, N. P.; Patel, H. A. Bioactive polymers: Synthesis, Release Study and Antimicrobial Properties of Polymer Bound Ampicillin. *Angew. Makromol. Chem.* **1999**, *271*, 24−27.
(28) Shi, Z.; Neoh, K.; Kang, E.; Poh, C.; Wang, W. Bacterial Adhesion and Osteoblast Function on Titanium with Surface-Grafted Chitosan and Immobilized RGD Peptide. *J. Biomed. Mater. Res., Part A* **2008**, *86*, 865−872.
(29) Kazemzadeh-Narbat, M.; Kindrachuk, J.; Duan, K.; Jenssen, H.; Hancock, R. E.; Wang, R. Antimicrobial Peptides on Calcium Phosphate-Coated Titanium for the Prevention of Implant-Associated Infections. *Biomaterials* **2010**, *31*, 9519−9526.
(30) Cortizo, M. C.; Oberti, T. G.; Cortizo, M. S.; Cortizo, A. M.; de Mele, M. A. F. L. Chlorhexidine Delivery System from Titanium/Polybenzyl Acrylate Coating: Evaluation of Cytotoxicity and Early Bacterial Adhesion. *J. Dent.* **2012**, *40*, 329−337.
(31) Zhang, F.; Zhang, Z.; Zhu, X.; Kang, E.-T.; Neoh, K.-G. Silk-Functionalized Titanium Surfaces for Enhancing Ssteoblast Functions and Reducing Bacterial Adhesion. *Biomaterials* **2008**, *29*, 4751−4759.
(32) Zheng, Y.; Li, J.; Liu, X.; Sun, J. Antimicrobial and Osteogenic Effect of Ag-Implanted Titanium with a Nanostructured Surface. *Int. J. Nanomed.* **2012**, *7*, 875.
(33) Liu, X.; Mou, Y.; Wu, S.; Man, H. Synthesis of Silver-Incorporated Hydroxyapatite Nanocomposites for Antimicrobial Implant Coatings. *Appl. Surf. Sci.* **2013**, *273*, 748−757.
(34) Jin, J.-C.; Xu, Z.-Q.; Dong, P.; Lai, L.; Lan, J.-Y.; Jiang, F.-L.; Liu, Y. One-step Synthesis of Silver Nanoparticles Using Carbon dots as Reducing and Stabilizing Agents and Their Antibacterial Mechanisms. *Carbon* **2015**, *94*, 129−141.
(35) Dos Santos, C. A.; Seckler, M. M.; Ingle, A. P.; Gupta, I.; Galdiero, S.; Galdiero, M.; Gade, A.; Rai, M. Silver Nanoparticles: Therapeutical Uses, Toxicity, and Safety Issues. *J. Pharm. Sci.* **2014**, *103*, 1931−1944.
(36) Chernousova, S.; Epple, M. Silver as Antibacterial Agent: Ion, Nanoparticle, and Metal. *Angew. Chem., Int. Ed.* **2013**, *52*, 1636−1653.
(37) Huang, Y.; Li, X.; Liao, Z.; Zhang, G.; Liu, Q.; Tang, J.; Peng, Y.; Liu, X.; Luo, Q. A Randomized Comparative Trial Between Acticoat and SD-Ag in the Treatment of Residual Burn Wounds, Including Safety Analysis. *Burns* **200**733, 161−166.10.1016/j.burns.2006.06.020
(38) Cao, H.; Liu, X.; Meng, F.; Chu, P. K. Biological Actions of Silver Nanoparticles Embedded in Titanium Controlled by Micro-Galvanic Effects. *Biomaterials* **2011**, *32*, 693−705.
(39) Ferraris, S.; Spriano, S. Antibacterial Titanium Surfaces for Medical Implants. *Mater. Sci. Eng., C* **2016**, *61*, 965−978.
(40) Cao, H.; Qiao, Y.; Liu, X.; Lu, T.; Cui, T.; Meng, F.; Chu, P. K. Electron Storage Mediated Dark Antibacterial Action of Bound Silver Nanoparticles: Smaller is not Aways Better. *Acta Biomater.* **2013**, *9*, 5100−5110.
(41) Necula, B.; Apachitei, I.; Tichelaar, F.; Fratila-Apachitei, L.; Duszczyk, J. An Electron Microscopical Study on the Growth of TiO_2−Ag Antibacterial Coatings on Ti6Al7Nb Biomedical Alloy. *Acta Biomater.* **2011**, *7*, 2751−2757.
(42) Yu, B.; Leung, K. M.; Guo, Q.; Lau, W. M.; Yang, J. Synthesis of Ag−TiO2 Composite Nano Thin Film for Antimicrobial Application. *Nanotechnology* **2011**, *22*, 115603.
(43) Meng, F.; Sun, Z. A Mechanism for Enhanced Hydrophilicity of Silver Nanoparticles Modified TiO_2 Thin Films Deposited by RF Magnetron Sputtering. *Appl. Surf. Sci.* **2009**, *255*, 6715−6720.
(44) Fielding, G. A.; Roy, M.; Bandyopadhyay, A.; Bose, S. Antibacterial and Biological Characteristics of Silver Containing and Strontium Doped Plasma Sprayed Hydroxyapatite Coatings. *Acta Biomater.* **2012**, *8*, 3144−3152.
(45) Yang, X.; Gondikas, A. P.; Marinakos, S. M.; Auffan, M.; Liu, J.; Hsu-Kim, H.; Meyer, J. N. Mechanism of Silver Nanoparticle Toxicity is Dependent on Dissolved Silver and Surface Coating in Caenorhabditis Elegans. *Environ. Sci. Technol.* **2012**, *46*, 1119−1127.
(46) Xiu, Z.-m.; Zhang, Q.-b.; Puppala, H. L.; Colvin, V. L.; Alvarez, P. J. Negligible Particle-Specific Antibacterial Activity of Silver Nanoparticles. *Nano Lett.* **2012**, *12*, 4271−4275.
(47) Lee, J. S.; Murphy, W. L. Functionalizing Calcium Phosphate Biomaterials with Antibacterial Silver Particles. *Adv. Mater.* **2013**, *25*, 1173−1179.
(48) Webb, K.; Hlady, V.; Tresco, P. A. Relative Importance of Surface Wettability and Charged Functional Groups on NIH3T3 Fibroblast Attachment, Spreading, and Cytoskeletal Organization. *J. Biomed. Mater. Res.* **1998**, *41*, 422.
(49) Shi, X.; Nakagawa, M.; Kawachi, G.; Xu, L.; Ishikawa, K. Surface Modification of Titanium by Hydrothermal Treatment in Mg-containing Solution and Early Osteoblast Responses. *J. Mater. Sci.: Mater. Med.* **2012**, *23*, 1281−1290.
(50) Wang, Q.; Zhang, Y.; Yang, K.; Tan, L. Preparation of Bioactive Film on Ti6Al4V. *Surf. Rev. Lett.* **2009**, *16*, 775−779.
(51) Kokubo, T.; Takadama, H. How Useful is SBF in Predicting in Vivo Bone Bioactivity? *Biomaterials* **2006**, *27*, 2907−2915.
(52) Feng, Q.; Wu, J.; Chen, G.; Cui, F.; Kim, T.; Kim, J. A mechanistic Study of the Antibacterial Effect of Silver Ions on Escherichia coli and Staphylococcus aureus. *J. Biomed. Mater. Res.* **2000**, *52*, 662−668.
(53) Ritger, P. L.; Peppas, N. A. A Simple Equation for Description of Solute Release II. Fickian and Anomalous Release From Swellable Devices. *J. Controlled Release* **1987**, *5*, 37−42.

DOI: 10.1021/acsami.6b04161
ACS Appl. Mater. Interfaces 2016, 8, 16584−16594

(54) Jamuna-Thevi, K.; Bakar, S.; Ibrahim, S.; Shahab, N.; Toff, M. Quantification of Silver ion Release, in Vitro Cytotoxicity and Antibacterial Properties of Nanostuctured Ag doped TiO2 Coatings on Stainless Steel Deposited by RF Magnetron Sputtering. *Vacuum* **2011**, *86*, 235−241.
(55) Xiu, Z.-M.; Ma, J.; Alvarez, P. J. Differential Effect of Common Ligands and Molecular Oxygen on Antimicrobial Activity of Silver Nanoparticles versus Silver Ions. *Environ. Sci. Technol.* **2011**, *45*, 9003−9008.
(56) Horzum, N.; Boyacı, E.; Eroglu, A. E.; Shahwan, T.; Demir, M. M. Sorption Efficiency of Chitosan Nanofibers toward Metal Ions at Low Concentrations. *Biomacromolecules* **2010**, *11* (12), 3301−3308.
(57) Jia, Z.; Xiu, P.; Li, M.; Xu, X.; Shi, Y.; Cheng, Y.; Wei, S.; Zheng, Y.; Xi, T.; Cai, H. Bioinspired Anchoring AgNPs onto Micro-nanoporous TiO_2 Orthopedic Coatings: Trap-killing of Bacteria, Surface-Regulated Osteoblast Functions and Host Responses. *Biomaterials* **2016**, *75*, 203−222.

DOI: 10.1021/acsami.6b04161
ACS Appl. Mater. Interfaces 2016, 8, 16584−16594

Supporting Information

Antibacterial Activity of Silver doped Titanate Nanowires on Ti Implants

Ziqiang Xu[b#], Man Li[b#], Xia Li[b], Xiangmei Liu [b]*, Fei. Ma [a], Shuilin Wu [b]*, K.W. K. Yeung[c], Yong Han [a]*, Paul K Chu [d]

[a] *State Key Laboratory for Mechanical Behavior of Materials，School of Materials Science and Engineering, Xi'an Jiaotong University*

[b] *Hubei Collaborative Innovation Center for Advanced Organic Chemical Materials, Ministry-of-Education Key Laboratory for the Green Preparation and Application of Functional Materials, Hubei Key Laboratory of Polymer Materials, School of Materials Science & Engineering, Hubei University, Wuhan, China*

[c]*Division of Spine Surgery, Department of Orthopaedics & Traumatology, Li Ka Shing Faculty of Medicine, The University of Hong Kong, Hong Kong, China*

[d]*Department of Physics & Materials Science, City University of Hong Kong, Tat Chee Avenue, Kowloon, Hong Kong, China*

These two authors contributed equally to this work.

* To whom correspondence should be addressed:

E-mail: shuilin.wu@gmail.com; shuilin.wu@hubu.edu.cn (S.L. Wu); yonghan@mail.xjtu.edu.cn (Y. Han)

Tel: +86-27-88661729 and Fax: +86-27-88665610 (SL Wu)

Table of contents in supporting information

Table S1 Contact angle values of prepared samples surfaces

	MP Ti	C-0.2	C-0.5	C-1	C-2.5
Angles (°)	63.3	9.6	10.4	14.7	2.7

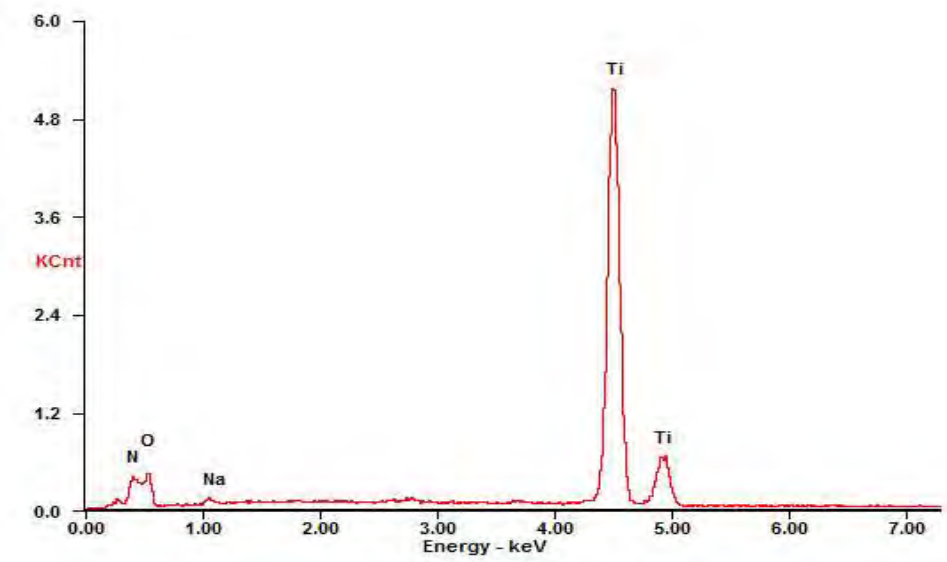

Figure S1. EDS spectrum of TNWs.

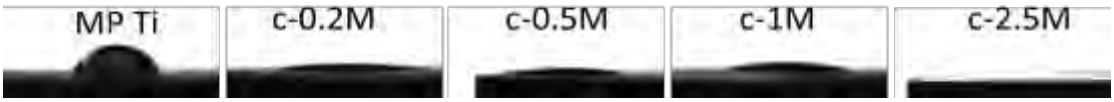

Figure S2. Images of water droplets lying on MP-Ti and TNWs modified Ti plates

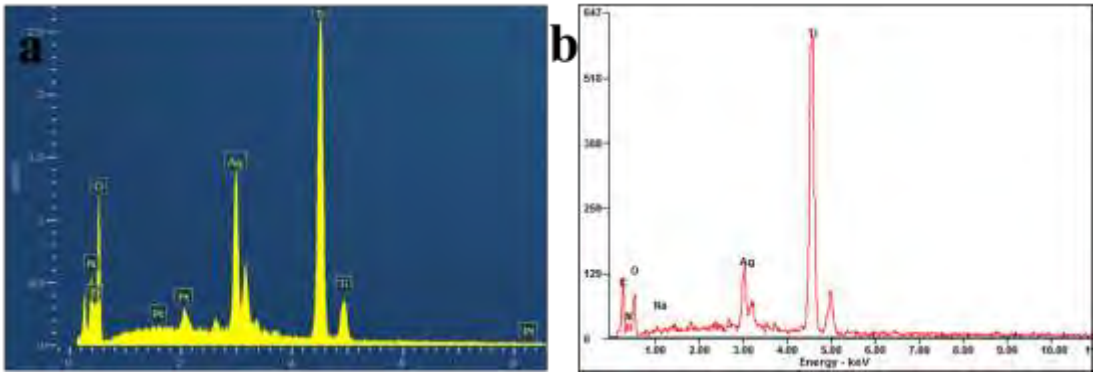

Figure S3. EDS spectra Ag doped (a) and Ag/CS capped TNWs (b).

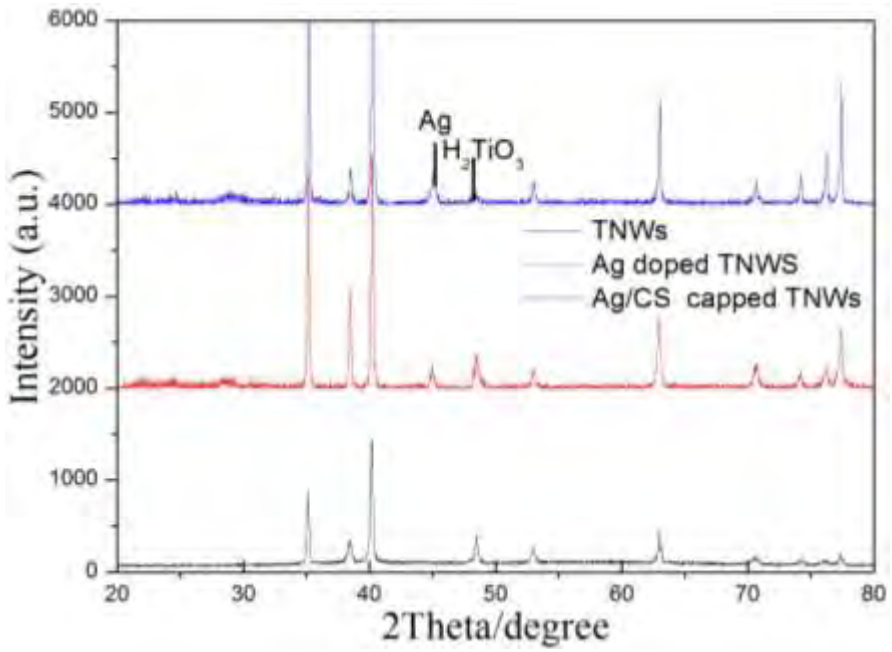

Figure S4. XRD spectra of TNWs, Ag doped and Ag/CS capped TNWs

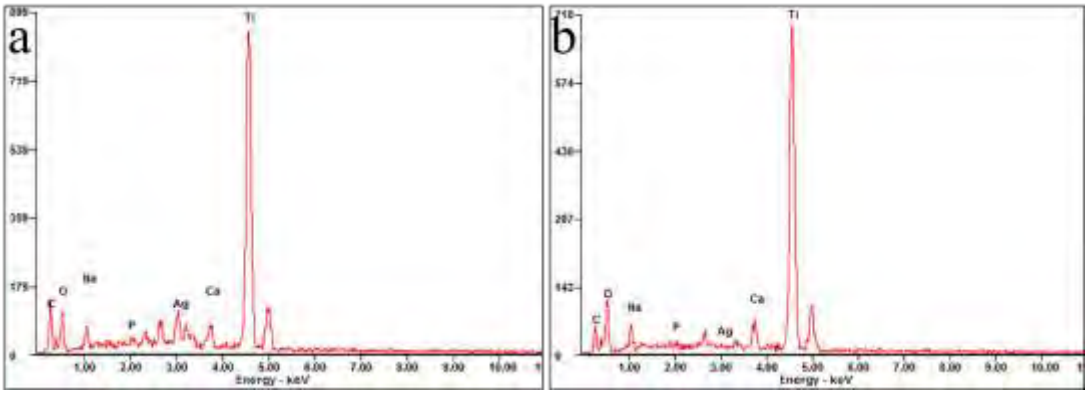

Figure S5 EDS spectra of (a) Ag doped TNWs, and (b) Ag/CS capped TNWs soaked in SBF for 14 Days.

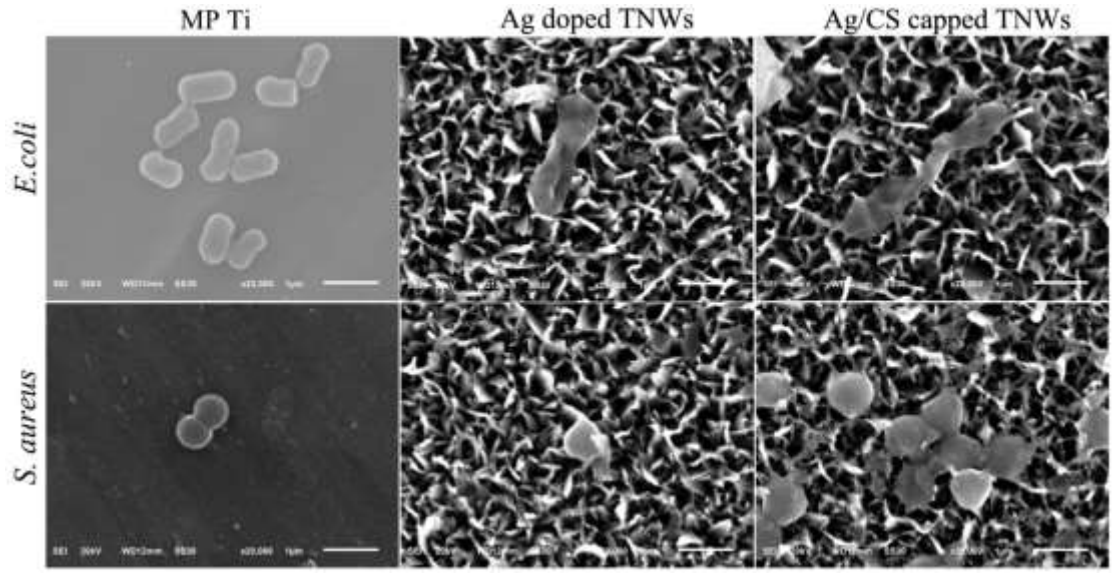

Figure S6. The morphologies of the *E. coli* and *S. aureus* attached on the MP Ti, Ag doped TNWs and Ag/CS capped TNWs.

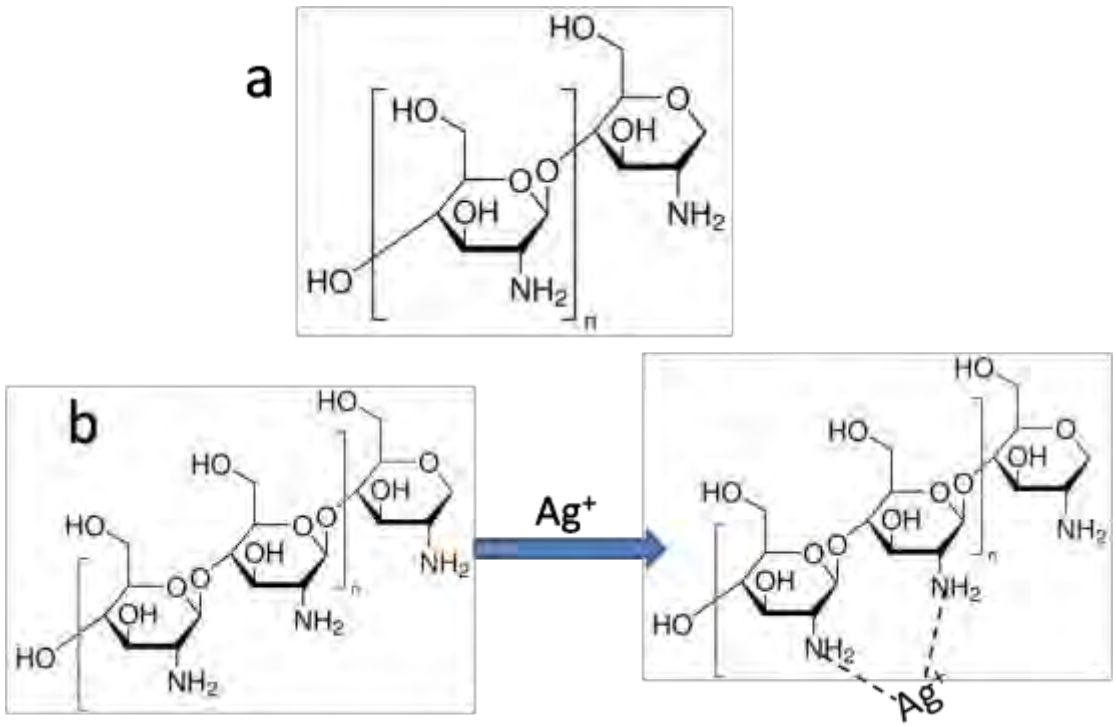

Figure S7. The molecular structure of CS (a). The scheme for coordination process of CS to Ag^{+}.

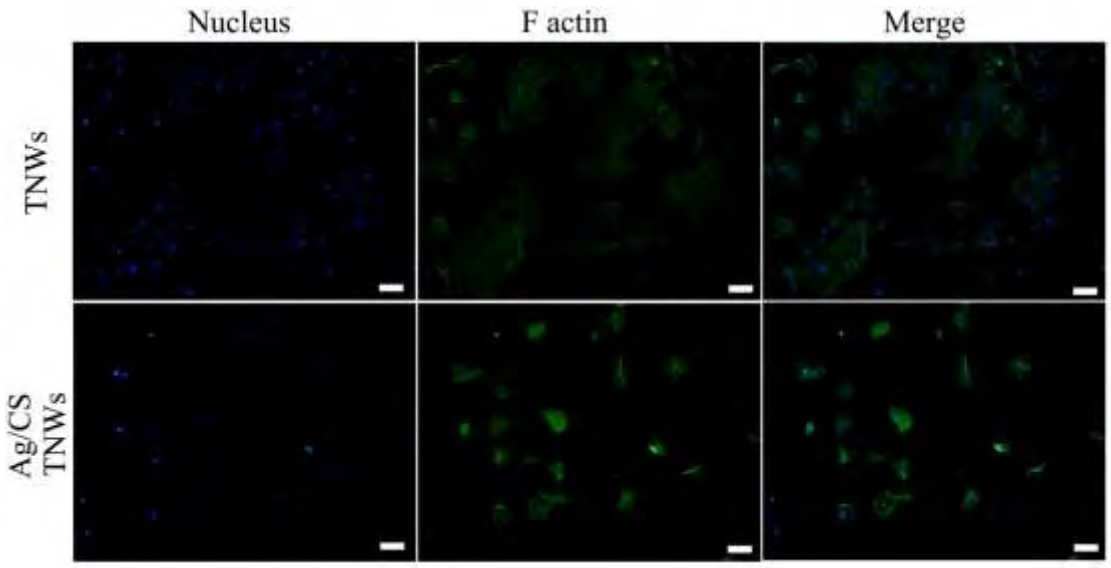

Figure S8. Fluorescent images of MC3T3 cells cultured on TNWs and Ag/CS TNWs for 24 h (scale bar: 100 μm).